PASJ: Publ. Astron. Soc. Japan **48**, 389–394 (1996)

Detection of Hard X-ray Emission in Mkn 463

Shiro UENO, Katsuji KOYAMA, Hisamitsu AWAKI, Ichizo HAYASHI
Department of Physics, Kyoto University, Sakyo-ku, Kyoto 606-01
E-mail (SU) ueno@cr.scphys.kyoto-u.ac.jp
and
Philip R. BLANCO
Center for Astrophysics & Space Sciences, University of California San Diego, La Jolla, CA 92093-0111, U.S.A.

(Received 1995 September 4; accepted 1996 March 18)

Abstract

We present the results of ASCA observations of the Seyfert galaxy Mkn 463. We find that the 1–10 keV X-ray spectrum consists of at least two components: soft and hard. We found no evidence for a strong Fe-K fluorescent line (equivalent width <670 eV). The soft component dominates below 4 keV and has a steep slope; the 0.2–4 keV flux is consistent with that determined from Einstein observations. It would appear that this soft X-ray emission comes from a distinct thermal component. The hard component, which has been detected for the first time by ASCA, is found only above 4 keV with an apparent flat spectral slope. We argue that most of these hard X-rays are likely coming directly from the nucleus of Mkn 463E, suffering a heavy absorption along our line of sight. For an assumed typical photon index of 1.7, the absorption column and intrinsic luminosity are estimated to be $(2.5 \pm 0.5) \times 10^{23}$ H cm^{-2} and 1×10^{43} erg s^{-1}. This hard X-ray luminosity is much less than that expected on the basis of Mkn 463E's optical and infrared properties.

Key words: Galaxies: active — Galaxies: individual (Mkn 463) — Galaxies: nuclei — X-rays: galaxies

1. Introduction

Mkn 463 is a distorted pair of interacting galaxies with a redshift of 0.0506 (Wills et al. 1977), containing two nuclei separated by about 4 arcsec on an east–west line.

The western nucleus (Mkn 463W) has a stellar continuum and narrow emission lines with FWHM of about 500 km s^{-1} (Wills et al. 1977; Hutchings, Neff 1989; Blanco 1991). Shuder and Osterbrock (1981) classified Mkn 463W as a Seyfert 2 by using the line flux ratio of [OIII]λ5007Å/Hβ. However, Wills et al. (1977) and Hutchings and Neff (1989) pointed out that the observed [OIII]/Hβ ratio is outside the typical range for Seyferts.

The eastern nucleus (Mkn 463E) shows a Type 2 Seyfert spectrum with emission line profiles having extended blue wings (Wills et al. 1977; Shuder, Osterbrock 1981; Hutchings, Neff 1989). Some well known indicators which support the presence of an obscured Seyfert 1 nucleus, as predicted by the unified model of Seyfert galaxies, have been found in Mkn 463E. Miller and Goodrich (1990) and Tran (1995) have detected broad Balmer lines in the polarized visible spectrum of Mkn 463E, and conclude that the light from a hidden Seyfert 1 is being scattered by electrons and/or dust into our line of sight. Mkn 463 also exhibits diffuse [OIII]λ5007Å emission extending about 20 arcsec north and south of the nuclei, roughly perpendicular to the position angle of the polarization of broad Balmer lines (Hutchings, Neff 1989). The [OIII] emission is considered to be related to radio activity in Mkn 463E (Hutchings, Neff 1989; Uomoto et al. 1993). Blanco (1991) found Seyfert 1-like features in the near-infrared band of Mkn 463E spectrum. Although Ginga observations of Mkn 463 gave only an upper limit of L(2-10keV)$< 4 \times 10^{43}$ erg s^{-1} (Awaki 1991), Mkn 463 has been detected at lower X-ray energies by the Einstein and ROSAT satellites; the Einstein observation of Mkn 463 gave a soft X-ray flux (0.2-4 keV) of 2×10^{-13}erg cm^{-2} s^{-1}(Kruper et al. 1990). The ROSAT flux (0.2–4 keV) is also 2×10^{-13}erg cm^{-2} s^{-1} (Blanco et al., in preparation).

From the far-infrared luminosity measured by IRAS, Mkn 463 was included in a sample of warm ($f_{25\mu m}/f_{60\mu m} > 0.2$) ultraluminous ($L(bol)\geq 10^{12} L_{\odot}$) galaxies by Sanders et al. (1988). These authors proposed that Mkn 463 is in the transition stage between cool ultraluminous IRAS galaxies and optical quasars. To date, only a few ultraluminous IRAS galaxies have been detected in the X-rays. We therefore observed Mkn 463 with ASCA to compare the X-ray spectrum of this interacting galaxy with normal Seyfert galaxies and investigate the spectral evolution hypothesis.

Throughout this paper we adopt a Hubble constant

Table 1. Sources in the GIS image selected by using a sliding-cell method*

Source	GIS 0.5-2keV (RA, DEC)$_{epock2000}$	GIS 4-10keV (RA, DEC)$_{epock2000}$	GIS 0.5-2keV 10^{-3}cnt/sec/GIS2+3‡	GIS 4-10keV 10^{-3}cnts/sec/GIS2+3‡	ID
A	209.034, 18.378†	209.022, 18.364†	7.5 ± 0.9	10.3 ± 1.0	Mkn463
B	209.256, 18.592	—	9.5 ± 1.4	< 5.5§	
C	208.890, 18.267	—	9.2 ± 1.8	< 6.0§	
D	209.136, 18.203	—	4.8 ± 1.4	< 5.6§	
E	209.138, 18.366	—	3.0 ± 0.7	< 2.2§	

* The criteria for the source detection are 1) the probability that the excess in each cell is due to a background fluctuation is less than 10^{-4}, and 2) the signal-to-noise ratio is larger than 3. Source A, B, and C have X-ray peaks in the Einstein IPC image obtained in 1979 January 24 (Harris et al. 1990). Source A, B, and D have peaks in the ROSAT PSPC image obtained in 1992 Jan 15.
† Difference in position between two energy bands is within the uncertainty for GIS.
‡ Observed counts are corrected for vignetting effects and for the fraction of the source counts that fall outside the box where the net counts are estimated.
§ 3σ upper limits evaluated at the soft-band positions.

$H_0 = 50\,\mathrm{km\,s^{-1}\,Mpc^{-1}}$.

2. Observations and Data reduction

The ASCA observations of Mkn 463 were performed on 1994 January 31 with the two Solid-state Imaging Spectrometers (SIS0 and SIS1) and the two Gas Imaging Spectrometers (GIS2 and GIS3). A summary of the ASCA mission and focal-plane detectors is found in Tanaka et al. (1994).

We rejected data obtained under high background environments, retaining only those portions of the data which satisfied the following selection criteria: 1) the elevation angle from the Earth edge was greater than 15 degrees, 2) the cut-off rigidity was higher than 6 GeV/c, and 3) the satellite was outside the South Atlantic Anomaly region. After this data selection, the remaining effective exposure time was about 36 ks.

3. Analysis and Results

Mkn 463 is the brightest source in the GIS and SIS fields of view. The broad-band GIS image (with a field of view of about 25 arcmin in radius) contains four obvious sources in addition to Mkn 463 (table 1). However in the (hard) 4–10 keV band image, only Mkn 463 is visible.

We extracted X-ray spectra for each detector from a circular region centered on Mkn 463. The extraction radii were 3 arcmin for GIS2 and GIS3, 3.4 arcmin for SIS0, and 2.7 arcmin for SIS1 (the radii for two SISs were limited by the gaps between the mosaiced CCD chips). We also extracted background spectra from off-source regions in the same field of view. From these we produced combined SIS (SIS0+SIS1) and GIS (GIS2+GIS3) spectra. Both of these combined spectra were then binned so that each energy bin contained at least 40 counts before background subtraction. For the spectral analysis presented below, we fitted these two combined spectra simultaneously.

We attempted to fit the data with single-component models modified by absorption in cold gas of solar abundances (Morrison, McCammon 1983): a power-law, and a single-temperature Raymond-Smith (RS) plasma with variable abundances (Raymond, Smith 1977). Both of these single-component models were rejected with reduced $\chi^2 > 2.8$ for 41 of degree of freedom (dof). The best fit photon index was 0.9 ± 0.1 for the power law model, and the best-fit RS temperature is > 60 keV (hereafter errors are given at 90% confidence level). Finding no evidence from these fits for local absorption ($N_H < 3.5 \times 10^{20}\,\mathrm{cm^{-2}}$), we fixed the absorption to the Galactic value corresponding to N_H of $2.09 \times 10^{20}\,\mathrm{cm^{-2}}$ (Kruper et al. 1990). In figure 1, the best-fit function of a single power law model and residuals from the data are shown. In the residuals, we find broad features at both the low- and high-energy ends; hence we examined two-component models.

We therefore fitted the spectra with two power-law components plus the Galactic absorption (Double power-law model in table 2). This model is only marginally consistent with the data; the best-fit reduced $\chi^2 = 1.7$ for 40 dof. The soft band (<3 keV) of the spectrum is best fitted by a power law of the photon index of 3.2 ± 0.5, and the hard band by a photon index of -0.3 ± 0.4. The soft band was equally fitted with thermal models; replacing the soft-band power law with an RS model, for example, gave a best-fit $kT = 0.56 \pm 0.14$ keV with abundance < 0.3 solar, while the hard-band power law index remained essentially unchanged. Thus regardless of the origin of

Table 2. Spectral fitting results with double-component models

Model	Component 1		Component 2		
	Parameter	Value	Parameter	Value	χ^2/dof
Double Power-Law model..	$\Gamma_{\rm ph}$	3.2 ± 0.5	$\Gamma_{\rm ph}$	-0.3 ± 0.4	68/40
	$N_H(10^{20}{\rm cm}^{-2})$	2.09*	$N_H(10^{20}{\rm cm}^{-2})$	2.09*	
Reflected model.....	$\Gamma_{\rm ph}$	3.0 ± 0.4	$\Gamma_{\rm ph}^{\ddagger}$	1.8 ± 0.4	60/40
	$N_H(10^{20}{\rm cm}^{-2})$	2.09*	$N_H(10^{20}cm^{-2})$	2.09*	
	flux(0.5-2keV)§	1.2×10^{-13}	flux(0.5-2keV)	7×10^{-15}	
	flux(2-10keV)§	3×10^{-14}	flux(2-10keV)	4.9×10^{-13}	
			EW†(eV)	< 580	
Heavily absorbed model....	$\Gamma_{\rm ph}$	2.7 ± 0.3	$\Gamma_{\rm ph}$	1.4 ± 0.9	59/39
	$N_H(10^{20}cm^{-2})$	2.09*	$N_H(10^{23}cm^{-2})$	1.6 ± 0.8	
	flux(0.5-2keV)§	1.2×10^{-13}	flux(0.5-2keV)	5×10^{-17}	
	flux(2-10keV)§	5×10^{-14}	flux(2-10keV)	4.3×10^{-13}	
			EW†(eV)	< 670	

∗ Fixed at the Galactic absorption.
† 90% upper limit of the equivalent width of 6.1keV line(6.4 keV in the rest frame).
‡ Photon index before reflection.
§ In units of erg cm^{-2} s^{-1}.

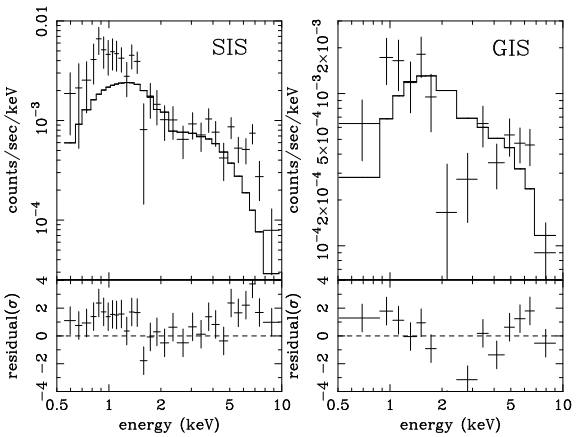

Fig. 1.. X-ray spectra of Mkn 463 and Single power-law model. Left panel: The SIS spectrum (SIS0+SIS1), Right panel: The GIS spectrum (GIS2+GIS3). Solid lines show a single power-law model, and the residuals are shown in lower panels.

the soft component, an extremely flat, hard continuum was required. The unusual flatness of this hard component, together with the marginal value of reduced χ^2, led us to examine other possibilities for the hard X-ray component, such as a heavily absorbed power law model and a reflection model (Lightman, White 1988). In these models, the apparent slope in the hard X-ray band may be flattened due to photo-absorption in cold material.

First we tried to fit the hard portion with the reflection model (Reflected model in table 2). As described in Lightman and White (1988), a photons hitting cold matter are reprocessed by photoelectric absorption and Compton down-scattering, into reflected emission with a flatter spectral shape than the incident spectrum. For realistic geometries, the direct power-law and the reflection components should be mixed together. However, we examined first the extreme case of a pure reflected component. The other extreme, which we examine later, is the heavy-absorbed power-law model, where only the direct component is included. We have fixed the solid angle sustained by the reflecting disk to 2π steradian, and the inclination angle of the disk to zero. Additional Galactic absorption was applied to these model spectra. The reflection model gave the photon index of incident spectrum of 1.8 ± 0.4 with the best-fit reduced χ^2 of 1.5 for 40 dof. In this case, the best-fit photon index for the soft component was derived to be 3.0 ± 0.4. Next, we tried the heavily absorbed power law model (Heavily absorbed model in table 2), adding a new parameter N_H for the absorption of the hard component. The best-fit N_H and photon index were found to be $(1.6 \pm 0.8) \times 10^{23}\,{\rm cm}^{-2}$ and 1.4 ± 0.9 respectively, with a reduced χ^2 of 1.5 for 39 dof. Since the fitted N_H and photon index are coupled to each other, we show confidence contours of these two parameters in figure 2. Fixing the photon index to be 1.7 (a typical value for Seyfert galaxies), the corresponding best-fit N_H is $(1.8 \pm 0.4) \times 10^{23}\,{\rm cm}^{-2}$, with a reduced χ^2 of 1.5 for 40 dof. The best-fit parameters of the soft component did not change within the errors. The resulting spectral model is shown in figure 3.

Our ASCA observations place limits on the presence of the 6.4keV Fe K emission line, which has been observed in many AGN. At the redshifted energy of 6.1keV we

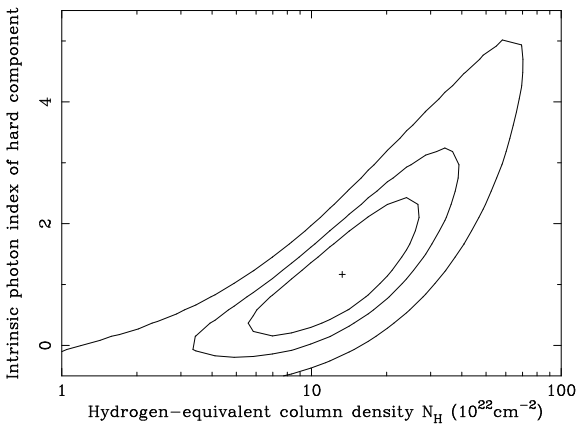

Fig. 2.. Confidence contours of the column density versus the intrinsic photon index for the hard component at the confidence levels of 68, 90, 99 %.

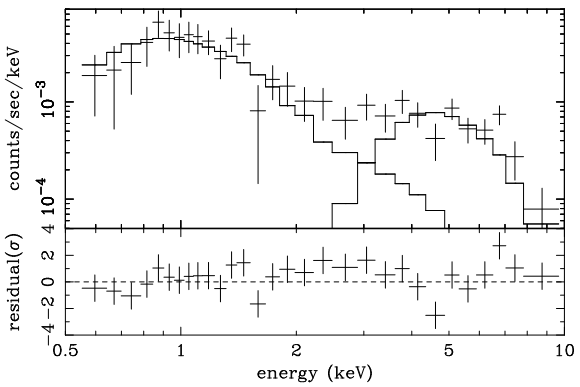

Fig. 3.. X-ray spectrum of Mkn 463 and double power-law model. The model was fitted with the SIS and GIS data simultaneously. Only the SIS data are shown. The solid lines are the best-fit model functions.
The photon index of the hard component is fixed at the value of 1.7.

found upper limits to the equivalent width of 580 eV for the reflected model and 670 eV for the absorbed power-law model at the 90% confidence level.

We also searched for evidence for X-ray variability in the SIS0, the SIS1, the GIS2, and the GIS3 data. We constructed X-ray light curves for the 0.5–4 keV and the 4–10 keV bands with a bin size of 256 s and applied the χ^2 test to the hypothesis of constant fluxes. The reduced χ^2 values were found to be equal to or less than about one (each for about 100 dof) for the soft and hard bands of all detectors. Thus no significant time variability was found over time scales of 10^3 s to 10 hr.

4. Discussion

4.1. Soft Component

The soft component can be reproduced by either power-law or by thermal models showing no significant line features. While a more detailed analysis of this component will be made in a future paper incorporating ROSAT data, we note here that (i) the ROSAT source is coincident with Mkn 463E, and (ii) we see no evidence of variability around 1 keV between the observations by Einstein (1979 Jan 24: Kruper et al. 1990), ROSAT (1992 Jan 15) and the ASCA observations presented here.

Given the correspondence with Mkn 463(E) and the existence of scattered broad line emission (Miller, Goodrich 1990), we examined the possibility that the X-ray soft component is also scattered light from Mkn 463E. The luminosity can be explained by the scattering of about 5% of the hard component, with the assumption that the intrinsic photon index of the hard component extends to 0.5 keV. Constraining the hard- and soft-component slopes to be equal gave a best fit N_H of $(2.7 \pm 0.5) \times 10^{23}$ H cm^{-2} for the hard component, and a photon index of 2.6 ± 0.2 with a reduced χ^2 of 1.6 for 39 dof. Since the fit is poor and the best-fit spectral slope is rather steep for Seyfert galaxies, we prefer the alternative possibility that the X-ray soft component has a separate, probably thermal origin.

4.2. Hard Component

The two nuclei (Mkn 463E and Mkn 463W) cannot be resolved in the ASCA images; their 4-arcsec separation is smaller than the ASCA's spatial resolution and the accuracy of positional determination of ~1 arcmin. However, the ionizing luminosities of the 2 nuclei are vastly different as judged from their optical spectra. On the basis of [OIII] λ5007Å line strengths, for instance, Mkn 463E is brighter by a factor of about 20 (Tull et al. 1979; Uomoto et al. 1993). Thus we identify Mkn 463E as the origin of the hard X-ray flux.

Modelling the hard component with a simple power law, we found that this component has an extremely flat slope with a photon index of about -0.3. Since the flat slope cannot be explained by the intrinsic spectrum of any known X-ray sources, we suspect that this hard component is due to photoelectric absorption of an intrinsically steeper spectrum. From the reduced χ^2 values of our continuum fits we cannot judge whether the reflection model or absorbed model is more realistic for the origin of the hard component. Nevertheless, we can estimate the contribution of the reflection model using the equivalent width of the iron line, since an X-ray spectrum reflected or scattered by cold material is expected to produce a high equivalent width (~2 keV) fluorescent iron K-line, as seen in NGC1068 (Koyama et al. 1989; Marshall et al. 1993; Ueno et al. 1994). On the other hand, a direct X-ray spectrum transmitted through a column N_H of 1.6×10^{23} H cm^{-2} would produce an equivalent width of about 200 eV (Inoue 1985). Thus if we reasonably assume that the iron abundance is comparable to

solar in Mkn 463E, the upper limit for the fluorescent Fe K line (<670 eV) implies that the absorbed power-law contributes at least 70% of the hard component flux.

The fitted X-ray absorption of this hard component corresponds to a dust extinction of $A_V \simeq 90$ mag for a Galactic dust-to-gas ratio. This is far higher than estimates of the dust extinction, for instance the 9.7 μm silicate feature measured by Roche et al. (1991) implies $A_V \simeq 7$ mag. The discrepancy is easily explained either by the different extents of the infrared and X-ray emitting regions, or by a large column of dust-free gas along the line-of-sight to the X-ray source.

From the best-fit N_H for the photon index of 1.7 assumed above, we therefore derive an intrinsic 2–10 keV luminosity L_X for the hard power law source to be 1×10^{43} erg s^{-1}, very close to the upper limit obtained with the Ginga satellite (Awaki 1991).

Well-established correlations exist for unobscured Seyfert 1 galaxies between their 2–10 keV luminosity and their broad-line, [OIII] and far-infrared luminosities. For Mkn 463E, all these indicators predict a much higher hard X-ray luminosity that we report here. We consider the far-infrared emission of Mkn 463, which is due mostly to Mkn 463E (Roche et al. 1991). Using the correlation presented by Ward et al. (1988) or Mulchaey et al. (1994) between L_X and infrared luminosity L_{IR} for Seyfert 1s, Mkn 463E's far-infrared luminosity of 3.4×10^{45} erg s^{-1} predicts $L_X \simeq 10^{44}$ erg s^{-1}. Similarly, the [OIII] luminosity of 4.1×10^{42} erg s^{-1} (Shuder, Osterbrock 1981; Mazzarella, Boroson 1993) implies comparable values of L_X if Mkn 463E is a typical Seyfert 1 (Mulchaey et al. 1994). Finally, broad line emission from Mkn 463E has been detected in the near-infrared by Blanco (1991) and Goodrich et al. (1994); these broad infrared lines may either be transmitted from the BLR, or reflected by a scattering region obscured by $A_V \simeq 5$ mag. In either case, using Mkn 463E's broad Paschen α flux of 1.9×10^{-13} erg cm^{-2} s^{-1} (Blanco 1991), the corresponding $L(\mathrm{H}\alpha)$ of 2.1×10^{43} erg s^{-1} would imply $L_X \simeq 1.7 \times 10^{44}$ erg s^{-1} from the correlation between these quantities established for Seyfert 1s (Ward et al. 1988).

It appears therefore, that at least at the current epoch, Mkn 463E is underluminous in X-rays compared to our expectations for typical Seyfert galaxies. If we are seeing only a fraction of Mkn 463E's true hard X-ray luminosity, the source must be highly anisotropic. Alternatively, by analogy with NGC1068 it may be completely obscured; however for this latter case have already argued against an origin of the observed hard component in an electron-scattered AGN continuum (due to the high N_H and lack of Fe K emission). While more sensitive observations of Mkn 463, extending to higher energy, are needed to determine N_H and the intrinsic shape of the hard component independently, the ASCA observations presented here have demonstrated that Mkn 463E does *not* conform to the simplest interpretation of the unified scheme for Seyfert galaxies, despite the persuasive evidence gathered from lower energies. If similar objects to Mkn 463 share its property of X-ray quietness (cf. Rieke 1988), an extension of the unified model of Seyfert galaxies may be required to incorporate such a new class of AGN.

5. Summary

1. The ASCA spectra of Mkn 463 require at least two components: soft and hard. No evidence was found for a strong fluorescent iron K line (EW<670 eV).
2. The soft component can either be explained by a non-thermal (photon index=2.7) or a thermal continuum ($kT = 1$ keV), with no evidence for long-term variability. We suggest that the steep spectral slope makes it unlikely that this soft component is due to electron scattering of an intrinsic AGN continuum.
3. The hard component has extremely flat slope. This is interpreted to be due to heavy absorption and/or reflection of an intrinsic Seyfert 1 continuum. From the limits on iron equivalent width, we suggest that more than 70% of these X-rays are due to the heavily absorbed transmitted component. For a typical photon index of 1.7, the intrinsic N_H and luminosity of this continuum are respectively estimated to be 1.8×10^{23} cm^{-2} and 1×10^{43} erg s^{-1}.
4. This inferred intrinsic hard X-ray luminosity is much smaller than that expected by comparison with Seyfert 1s of comparable broad line, [OIII], and far-infrared luminosities. This implies that at least at the current epoch, Mkn 463E is an X-ray quiet AGN. Similar hard X-ray observations of other infrared-luminous Seyfert 2s will be able to establish whether this is a general property of this class of active galaxy.

We thank the ASCA operations, instrument development, and software teams who have made this study possible. P.R.B. is supported by NASA contract NAS5-30720.

References

Awaki H. 1991, Ph.D. thesis, Nagoya University
Blanco P. R., 1991, Ph.D. thesis, University of Edinburgh
Goodrich R. W., Veilleux S., Hill G. J., 1994, *ApJ*, **422**, 521
Harris D.E., Forman W., Gioia I.M., Hale J.A., Harnden Jr. F.R., Jones C., Karakashian T., Maccacaro T. et al. 1990, *Einstein Observatory Catalog of IPC X-Ray Sources*, **5**, 377
Hutchings J.B., Neff S.G. 1989,*AJ*,**97**,1306
Inoue H. 1985, *Space Sci. Rev.*,**40**, 317
Koyama K., Inoue H., Tanaka Y., Awaki H., Takano S., Ohashi T., Matsuoka M. 1989,*PASJ*,**41**, 731
Kruper J.S., Urry C.M., Canizares C.R 1990, *ApJS*,**74**, 347

Lightman A.P., White T.R. 1988,*ApJ*,**335**, 57
Mazzarella J.M., Gaume R.A., Soifer B.T., Graham J.R., Neugebauer G., Matthews K. 1991,*AJ*,**102**, 1241
Marshall F.E., Netzer H., Arnaud K.A., Boldt E.A., Holt S.S., Jahoda K.M., Kelley R., Mushotzky R.F. et al. 1993,*ApJ*,**405**,168
Miller J.S., Goodrich R.W. 1990,*ApJ*,**355**,456
Morrison R., McCammon D. 1983,*ApJ*,**270**,119
Mulchaey J. S., Koratkar A., Ward M. J., Wilson A. A., Whittle M., Antonucci R. R. J., Kinney A. L., Hurt T. 1994, *ApJ*, **436**, 586
Raymond J.C., Smith B.W. 1977, *ApJS*, **35**, 419
Rieke, G. H. 1988, *ApJL*, **331**, L5
Roche P. F., Aitken D. K., Smith C. H., Ward M. J. 1991, *MNRAS*, **248**, 606
Sanders, D.B., Soifer, B.T., Elias, J.H., Neugebauer, G., Matthews, K. 1988, *ApJ*, **328**, L35
Shuder J.M., Osterbrock D.E. 1981, *ApJ*, **250**, 55
Tanaka Y., Inoue H., Holt S.S. 1994, *PASJ*, **46**, L37
Tran, H. D. 1995, *ApJ*, **440**, 578
Tull R.G., Vogt S.S., Kelton P.W. 1979, *Instr. Astr. III, SPIE Proc.*, **172**, 90
Ueno S., Mushotzky R.F., Koyama K., Iwasawa K., Awaki H., Hayashi I. 1994, *PASJ*, **46**, L71
Uomoto A., Caganoff S., Ford H.C., Rosenblatt E.I., Antonucci R.R.J., Evans I.N., Cohen R.D. 1993,*AJ*,**105**,1308
Ward M.J., Done C., Fabian A.C., Tennant A.F., Shafer R.A. 1988, *ApJ*, **324**, 767
Wills B.J., et al. 1977, *BAAS*, **9**, 647